ACS APPLIED MATERIALS & INTERFACES

Research Article

www.acsami.org

Highly Active Biocatalytic Coatings from Protein–Polymer Diblock Copolymers

Aaron Huang, Guokui Qin, and Bradley D. Olsen*

Department of Chemical Engineering, Massachusetts Institute of Technology, 77 Massachusetts Avenue, Cambridge, Massachusetts 02139, United States

Supporting Information

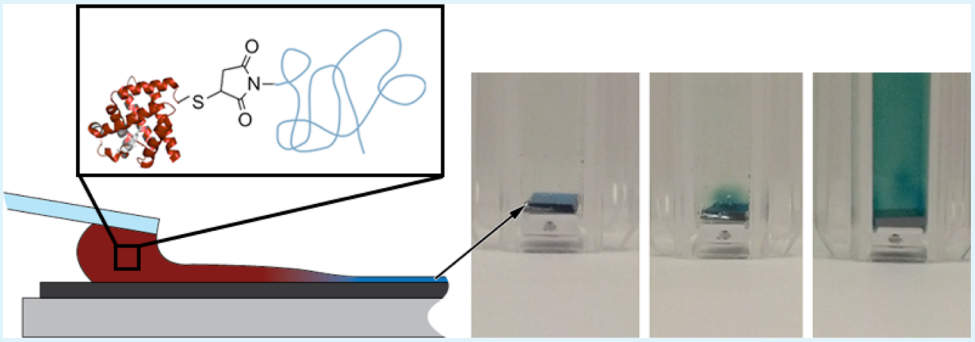

ABSTRACT: A method for fabricating nanostructured biocatalysts using bioconjugate block copolymer self-assembly is demonstrated, yielding very high protein loadings and activity per unit area, compared to more-established enzyme encapsulation methods. Self-assembled heterogeneous biocatalysts are fabricated by flow coating myoglobin-*b*-poly(*N*-isopropylacrylamide) (myoglobin-PNIPAM) block copolymers onto solid supports, and films are stabilized by lightly cross-linking with glutaraldehyde. The conjugates form weakly ordered, nonbirefringent micellar and lamellar assemblies in concentrated solution and disordered but micro-phase-separated structures in thin solid films. The low diffusion resistance in the bioconjugate film imparted by the water-swollen PNIPAM nanostructures, the high enzyme density within the film, and high retention of protein activity results in extremely high catalytic activity: 5–10 times greater than catalysts fabricated using other well-established methods.

KEYWORDS: *biocatalyst, block copolymer, myoglobin, bioconjugation*

INTRODUCTION

Biocatalysts provide selective, efficient, and renewable pathways to carry out a variety of industrially and medically relevant reactions for biofuel synthesis,[1,2] carbon sequestration,[3,4] sensing and remediation of nerve agents,[5−7] glucose detection,[8,9] biofuel cells,[10] drug delivery,[11] and industrial reactions such as penicillin synthesis[12] or glucose-fructose isomerization.[13] Despite the usefulness of enzymes, they can often be expensive, particularly if the enzyme is difficult to isolate from natural sources or produce from recombinant sources. Unfortunately, the enzymes, which exist in homogeneous solution, are typically destroyed and discarded during post-reaction separation processes. As a result, strategies for extending the useable lifetime of an enzyme have attracted much attention.[14] In particular, incorporating the enzyme into heterogeneous biocatalysts allows for the reuse or recycling of the enzyme or the use of the enzyme in continuous processes,[15,16] dramatically expanding the practical applications of enzymatic catalysis. Therefore, the development of improved heterogeneous biocatalysts has the potential to have a large impact on decreasing costs for chemical syntheses and produce more efficient and sensitive bioelectrocatalysts/biosensors.

Numerous considerations must be taken into account when designing an effective heterogeneous biocatalyst.[17] The catalyst should enable rapid transport of the product and substrate or charge carriers to mitigate diffusion limitations. The material should also be structured in three dimensions to achieve a high surface density of active sites, and the enzyme should be oriented in such a way as to avoid hindering access to the active sites or co-factor binding sites. Finally, the material should maintain or extend the active lifespan of the enzyme as much as possible. Motivated by these design criteria, a variety of methods for enzyme immobilization have been developed.[16,18] Reactive residues on the protein such as the amines in lysine can be utilized to couple the enzyme to reactive moieties on a support,[19,20] histidine tags can ligate enzymes to Co^{2+} or Ni^{2+},[21] or the enzyme can be glycosylated and immobilized to hydrophilic carriers such as cellulose.[18,22] Many of these immobilization chemistries are readily combined with nanolithography to produce two-dimensional protein patterns on surfaces.[23,24] In addition to immobilizing enzyme via

Received: March 2, 2015
Accepted: May 21, 2015
Published: July 2, 2015

DOI: 10.1021/acsami.5b01884
ACS Appl. Mater. Interfaces 2015, 7, 14660–14669

interactions with a surface, techniques have also been developed to encapsulate enzymes. Common methods of encapsulating enzymes include forming capsules or films through layer-by-layer (LbL) assembly,[25,26] incorporating the enzyme into a bulk polymeric matrix such as a polyurethane,[5,27] or intercalating the enzyme within gels formed by micellar polymers.[16,28] These encapsulation techniques allow for straightforward control of the areal density of the enzyme by varying the thickness of the material.

Despite the diverse assortment of immobilization techniques, few offer control of the three-dimensional structure at the nanoscale that can simultaneously engineer transport properties and enzyme packing density. Block copolymer self-assembly provides an attractive mechanism to produce such biocatalytic nanostructures via self-assembly of periodic domains on a length scale of 5−100 nm.[29−32] Several groups have demonstrated the self-assembly of protein−polymer conjugates such as block copolymers into solid-state nanomaterials and gels or micellar nanostructures, while still retaining the protein fold.[33−37] However, replacing a Gaussian coil with a folded globular protein block significantly changes the phase behavior of the system, as a result of the defined shape of the protein.[38−42] Previous studies from our group have shown that, in a model conjugate such as mCherry-*b*-PNIPAM, the phase diagram is highly asymmetric, with cylinders predominantly observed at coil volume fractions below 0.5 and lamellae observed above.[42] Changing the polymer block results in large changes in the observed phase diagram and the presence of new nanostructures;[43] in contrast, mutations to surface residues on mCherry or the use of the alternative β-barrel enhanced green fluorescent protein (EGFP) results in only minor alternations in phase behavior.[37] These results suggest that polymer−protein interactions are very important for self-assembly, while the detailed surface potential of the protein is less important than its coarse-grained shape. Although this understanding of thermodynamics in these systems is still rapidly developing, the ability to control nanostructure via self-assembly of these bioconjugate block copolymers offers an attractive solution to the design of structured biocatalytic materials if enzymes can be incorporated.

In this work, the self-assembly of protein−polymer diblock copolymers is demonstrated as a method to achieve both efficient transport and high enzyme loading in enzymatic materials, producing biocatalytic coatings with an activity per area 5−10 times higher than comparable methods. Solid-state thin-film coatings are constructed from block copolymers composed of the model peroxidase human heart myoglobin (hMb) conjugated to a self-assembly directing polymer poly(*N*-isopropylacryamide) (PNIPAM). The temperature- and concentration-dependent phase behavior of this material is investigated, and the performance as a heterogeneous catalyst is quantified using reaction-diffusion models. Quantitative evaluation of the material against catalysts fabricated with commonly used enzyme immobilization methods demonstrates the potential of block copolymer self-assembly to make a large improvement in biocatalyst performance.

RESULTS AND DISCUSSION

Protein−Polymer Diblock Copolymer Design. Recombinant human heart myoglobin (hMb) was chosen as a model peroxidase,[44] representing a class of enzymes with broad substrate specificity and utility in catalyzing oxidation reactions.[45] As a result, developments made with this hMb can potentially be applied to several similar protein systems with analogous catalytic mechanisms.[46,47] hMb is a good model for catalyst design, because it has an established, easy to measure, colorimetric assay for determination of the enzymatic activity,[44] a known crystal structure,[48] and the enzyme itself has a characteristic optical absorption, because of the presence of the bound heme group that can be used to quantify the maintenance of a tertiary structure. Finally, the native sequence for hMb contains only a single cysteine residue at position 110, which has been determined to be noncritical to the structure and function of the enzyme.[49] This allowed for the cysteine to be replaced by alanine to form hMbC110A and then for a cysteine to be introduced at the N-terminus to provide a unique thiol residue for bioconjugation. The conjugation site was chosen so as not to significantly affect the activity of the enzyme. In addition, the conjugation site was chosen in an accessible location, allowing the hMb to be coupled via site-specific conjugation to the thermoresponsive polymer poly(*N*-isopropylacrylamide) (PNIPAM) which drives self-assembly. Although site-specific thiol-maleimide coupling is a convenient method for conjugating myoglobin to a synthetic polymer that can be broadly applied to many different proteins,[50,51] a variety of bioconjugation techniques have been and continue to be developed that can provide synthetic routes toward analogous bioconjugates for an even wider variety of enzymes.[39,52−54]

The hMb-PNIPAM conjugate was designed to have approximately equal masses of protein and PNIPAM, which has been previously shown to promote self-assembly at a minimum concentration.[41,43] Characterization data for the protein, polymer, and conjugate are summarized in Table 1.

Table 1. Characterization Data for the Protein, Polymer, and Conjugate

	molecular weight (Da)	polydispersity index	coil fraction
hMbC110A	19710		
PNIPAM	18880	1.095	
hMb-PNIPAM	38590		0.489

UV-vis absorption spectra (Figure S8 in the Supporting Information) and circular dichroism (Figure S9 in the Supporting Information) showed no change in the protein secondary or tertiary structure between the unconjugated hMbC110A and the hMb−PNIPAM conjugate. In addition, solution-phase enzymatic activity assays reveal a significant increase in the catalytic activity after conjugation (Figure 1). However, this perceived enhancement in activity upon conjugation of hMb is likely due to the bioconjugation blocking the reactive cysteine group present in the hMbC110A variant from side reactions with the assay product.[55] Nevertheless, the conjugate displays very similar activity to commercially available equine heart myoglobin (eMb) (Figure 1), indicating that the addition of the PNIPAM block does not hinder the transport of substrates, affect the protein fold, or interfere with the catalytic mechanism of hMb.

Self-Assembly in Bulk Gels and Thin Films. As observed with previously studied protein−polymer conjugates, hMb−PNIPAM self-assembles in concentrated solution and solid materials to form nanostructured phases that can meet the structural criteria for biocatalyst design. However, unlike previous studies on structurally similar mCherry and EGFP, the strongly dissimilar myoglobin shows large changes in its

DOI: 10.1021/acsami.5b01884
ACS Appl. Mater. Interfaces 2015, 7, 14660−14669

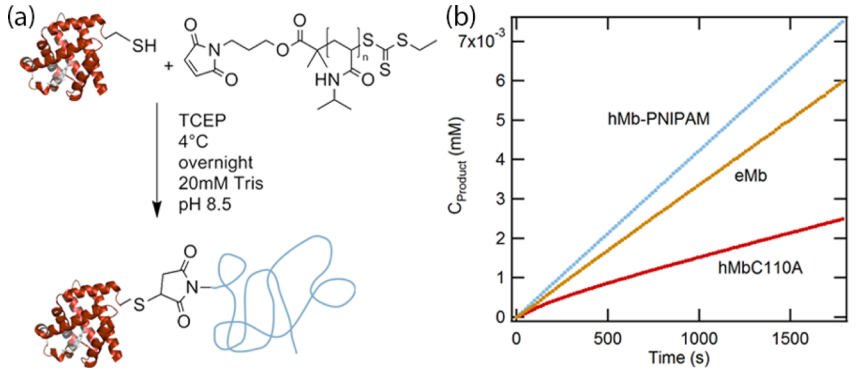

Figure 1. (a) hMb−PNIPAM bioconjugates are synthesized using thiol-maleimide coupling. (b) The resulting bioconjugate shows little difference in activity from the unconjugated enzyme by an ABTS/H_2O_2 assay.

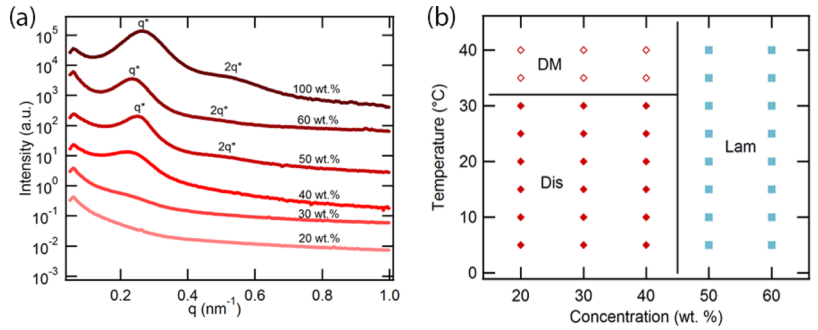

Figure 2. (a) Bulk solution phase SAXS patterns of hMb−PNIPAM at 25 °C show no ordering at low concentrations and weak ordering at concentrations of 50% and above. Curves are offset for the sake of clarity. (b) Phase diagram for hMb−PNIPAM. At concentrations of 40wt % and below, the conjugate micellizes at high temperature. At concentrations of 50 wt % and higher, the material assembles into disordered lamellar structures.

phase behavior. This clearly indicates that changes in protein structure can result in large effects on self-assembly. The degree of order in self-assembled myoglobin conjugates is significantly worse than well-characterized systems based on mCherry and EGFP, as demonstrated by small-angle X-ray scattering (SAXS) patterns for the hMb−PNIPAM conjugate taken over a range of concentrations and temperatures (see Figure 2, as well as Figure S10 in the Supporting Information). Consistent with observations made in previously studied globular protein−polymer conjugates containing mCherry and EGFP,[37,41] a disordered phase is observed at low temperature and low concentration. At 20 wt %, the strength of segregation in the hMb−PNIPAM is so weak that no peak is observed, whereas at 30 and 40 wt %, a broad peak is observed consistent with the disordered phase. At 50 wt %, microphase separation of the material can be observed as the concentration is increased above C_{ODT}, indicated by the primary peak narrowing and increasing intensity. At 50 and 60 wt %, a q^* peak and a weak $2q^*$ peak can be observed, evidencing a weakly ordered lamellar morphology with domain spacings of 25.0 nm at 50 wt % and 26.6 nm at 60 wt %. The increase in domain spacing with increasing concentration suggests increasing segregation between the protein and polymer blocks of the copolymer. Depolarized light scattering measurements of the solution phase samples showed no birefringence across the entire concentration range (see Figure S11 in the Supporting Information), which is consistent with the relatively poor degree of order in all of the samples observed by SAXS. When the sample is dried into the solid state, SAXS reveals a similar morphology to the 50 and 60 wt % samples with the q^* peak and $2q^*$ peak shifted slightly to the right, consistent with having a smaller domain spacing of 23.9 nm, because of dehydration of the nanostructures. The smaller domain spacing in the solid-state sample is a consequence of dehydration of the block copolymer nanostructures.

Heating the conjugates at a given concentration results in desolvation of the PNIPAM block and can potentially trigger a change in the nanostructured morphology. At low concentrations, where the material is disordered at low temperature, heating results in micellization of the block copolymer, as observed by a change in the SAXS pattern and the formation of an optically transmissive, nonbirefringent high-temperature phase (see Figure S11 in the Supporting Information). Differential scanning calorimetry (DSC) measurements indicate that these transitions occur at 33.3 °C at 20 wt %, 31.8 °C at 30 wt %, and 30.5 °C at 40 wt %. At concentrations of 50 and 60 wt %, there is no change observed with increasing temperature, indicating that crossing the PNIPAM thermal transition does not result in a change in the relatively disordered lamellar nanodomain structure at these lower water contents. A phase diagram for this conjugate is shown in Figure 2.

When compared with previously studied mCherry and EGFP systems, the hMb−PNIPAM conjugates show much weaker ordering at higher concentrations and no order−order transition at any of the concentrations tested. This result suggests that changes in protein structure can yield substantial changes in protein block copolymer self-assembly. Previously, it has been observed that the phase behavior of mCherry, EGFP, and mCherry mutants are very similar despite significant

DOI: 10.1021/acsami.5b01884
ACS Appl. Mater. Interfaces 2015, 7, 14660−14669

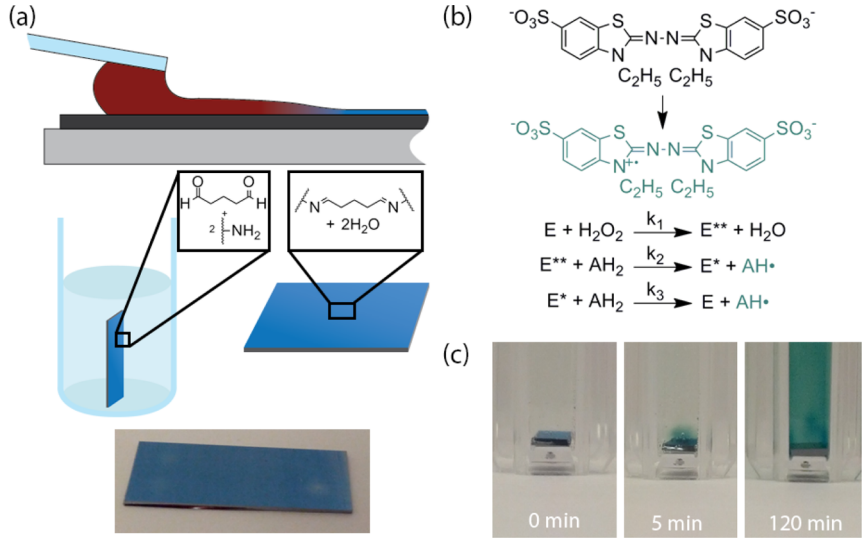

Figure 3. (a) hMb−PNIPAM bioconjugate is flow coated under a glass blade and cross-linked into a stable film using glutaraldehyde. (b) The peroxidase enzyme oxidizes ABTS in the presence of hydrogen peroxide. (c) The resulting radical exhibits an intense blue-green color in solution which can be measured spectrophotometrically at 414 nm. The high activity of the film results in rapid formation of a boundary layer in the absence of rapid stirring.

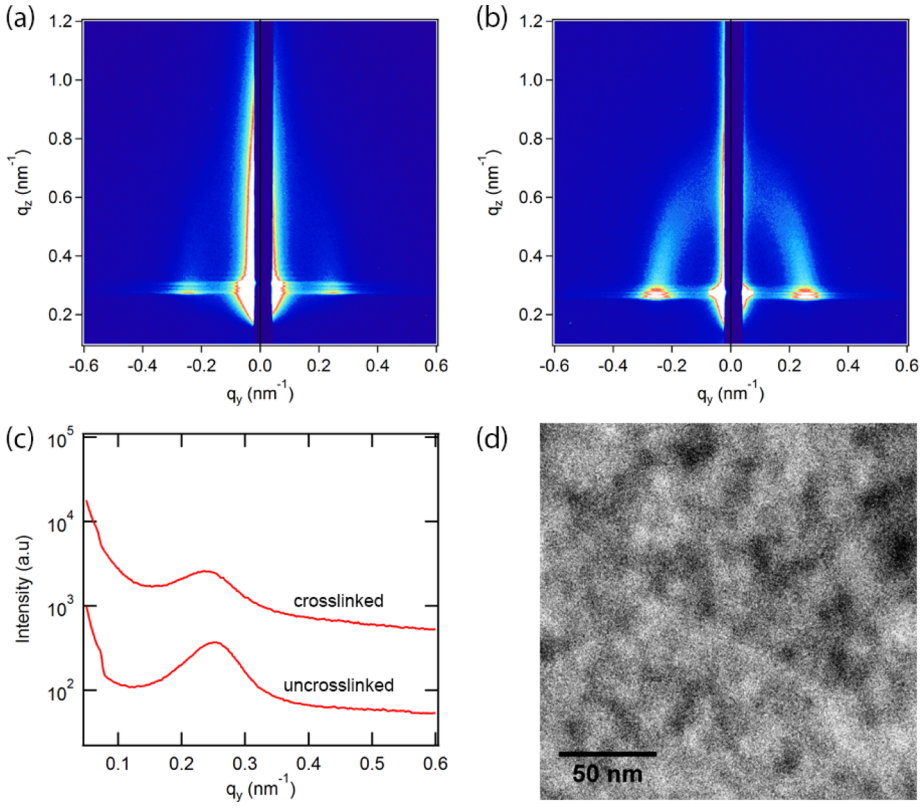

Figure 4. (a) GISAXS pattern for the cross-linked film taken at an incidence angle of 0.16°; (b) GISAXS pattern for the un-cross-linked film taken at an incidence angle of 0.16°; (c) integrated line cuts of the GISAXS patterns; and (d) TEM micrograph of hMb−PNIPAM film shows randomly connected, disordered domains. Dark regions correspond to hMb domains and light regions correspond to PNIPAM domains due to RuO_4 staining.

differences in electrostatic patchiness and amino acid sequence, indicating that proteins with similar size, shape, and virial coefficient undergo similar self-assembly.[37,41] These proteins are all structurally homologous, each having a β-barrel structure, and have similar second virial coefficients. However, the hMb is less symmetric, having a significantly different molecular shape, size, charge, and hydrophobicity. The irregularity in its shape may result in greater difficulty packing within ordered domains. This result clearly indicates that, for proteins with significant structural diversity, there can be a large impact of protein structure on self-assembly, which motivates a systematic study of these interactions in future systems.

In order to prepare heterogeneous biocatalysts, the conjugates must self-assemble in thin films. Catalytically active

DOI: 10.1021/acsami.5b01884
ACS Appl. Mater. Interfaces 2015, 7, 14660−14669

films of the hMb−PNIPAM were fabricated using a flow coater to deposit a thin film of the conjugate on a silicon support, according to the process illustrated in Figure 3.[56] Flow coating was selected as the film fabrication method, because it yields smooth, even films with minimal shear forces, which can result in a loss of protein activity. The dried film had a pale blue color, because of thin film interference, which is consistent with the 152 ± 5 nm thickness measured by ellipsometry. Little variation in thickness was measured over film areas of 20 cm^2. To stabilize the films against dissolution in water, the amine groups on the protein within the film were then cross-linked at 45 °C in a 1.4 wt % aqueous glutaraldehyde solution for 20 s, rinsed for 20 s in room-temperature DI water in order to remove any unbound conjugate, and dried under an air stream. The temperature of the glutaraldehyde solution was chosen to prevent the films from dissolving by taking advantage of the thermoresponsive properties of PNIPAM while minimizing denaturing of the enzyme that could occur at higher temperatures. Glutaraldehyde was used as a cross-linking agent, because it is a quick and effective method of cross-linking the protein domains. Although it cannot cross-link the polymer, cross-linking the protein domains imparts enough stability to prevent the film from disintegrating or delaminating from the surface. After cross-linking, the films were observed to be stable in water for longer than 10 days with no measurable change in film thickness by ellipsometry (see Figure S13 in the Supporting Information), to be mechanically stable enough to be rinsed under running deionized water without visible damage to the film surface or permanent change in the film thickness, and to reversibly change to a deep magenta color upon submersion in water, indicating a high degree of swelling to ∼460 nm.

In solid thin films, grazing-incidence small-angle X-ray scattering (GISAXS) shows that the conjugates form poorly ordered microphase separated structures during casting, similar to those formed in the solid state. The GISAXS patterns reveal a pronounced primary peak but no higher order peaks, indicating that the materials are microphase separated but lacking long-range order within the films. After gluteraldehyde cross-linking, the morphology of the film remains largely unchanged. The average domain spacing is 26 nm in the un-cross-linked film and 24 nm in the cross-linked film, which is close to the spacing found in the bulk, solid-state sample (Figure 4). Transmission electron microscopy (TEM) was used to verify microphase separation in the film. The same flow coating technique described above was used to coat a film on a silicon nitride TEM substrate. Contrast in the sample is improved by negatively staining the protein domains with ruthenium tetroxide, which selectively reacts with alcohol, amine, and aromatic moieties in the protein. In the bright-field micrograph (Figure 4), dark and light regions corresponding to the hMb and PNIPAM domains, respectively, are visible. Both scattering and microscopy show that the resulting film structures form highly disordered yet microphase-separated structures of protein and polymer. Although well-ordered arrays are not formed, these structures potentially offer the appropriate control over transport, because of the percolating domains of polymer, which can offer paths for rapid diffusion of the substrate through the catalyst.

Self-Assembled Heterogeneous Catalysts. The self-assembled myoglobin films remain highly active in the solid state, as illustrated in Figure 5, and the activity of the films does not diminish over five washes and reuses (see Figure S14 in the Supporting Information). The catalytic activity of the films was quantified using a 2,2′-azino-bis(3-ethylbenzothiazoline-6-sulfonic acid) (ABTS) peroxidase assay, which measures the conversion of ABTS into a stable blue-green $ABTS^{-\bullet}$ radical upon a peroxidase-catalyzed reaction with hydrogen peroxide. This catalytic cycle can be represented by the sequence of reactions outlined in Figure 3.

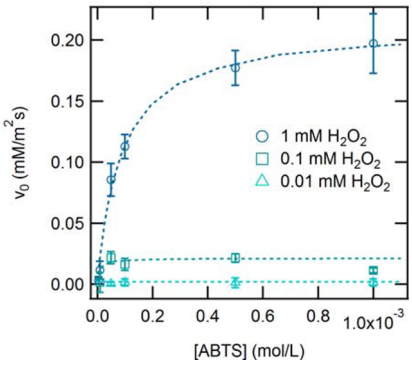

Figure 5. Enzymatic activity of the bioconjugate catalyst measured at various concentrations of ABTS and H_2O_2. Rates begin to plateau at ∼0.0005 mol/L ABTS, indicating a reaction limitation at higher concentrations. The dotted lines show that the Michaelis−Menten equation is a good approximation of the reaction kinetics.

In these heterogeneous catalysts, the reaction rate observed in solution is a consequence of reaction at the enzyme, as well as the diffusivity of the substrates and products within the catalyst film. Therefore, to characterize the activity of the catalyst and enable quantitative comparison, a reaction−diffusion model has been developed. The no-flux boundary condition (eq 2) at the interface between the solid support and bioconjugate film is used, and the Diriclet boundary condition (eq 3) at the interface between film and the reaction solution is assumed, because of rapid, vigorous stirring of the reaction solution. The general form of the reaction−diffusion equation and the boundary conditions are given below:

$$\frac{-\partial s}{\partial t} = D_s \nabla^2 s + R(s) \tag{1}$$

$$\left(\frac{\mathrm{d}s}{\mathrm{d}x}\right)_{x=0} = 0 \tag{2}$$

$$s(x = 1) = s_\infty \tag{3}$$

where D_s is the diffusion coefficient of the substrate within the film, s the substrate concentration, s_∞ the substrate concentration in the reaction solution, t the time, and x the position. $R(s)$ accounts for any reactions involving the substrate. In the planar film geometry, this equation can be simplified by assuming transport in one dimension and that the pseudo-steady-state approximation (PSSA) applies, because of the thinness of the film. For the catalytic cycle depicted in Figure 3, a Michaelis−Menten-like reaction equation can be expressed as follows, under the simplification that $k_3 \gg k_2$.[45]

$$\frac{-\mathrm{d}s}{\mathrm{d}t} = \frac{2k_3[E]s}{1 + \frac{k_3}{k_1[H_2O_2]}s} = \frac{ks}{1 + \frac{s}{K}} \tag{4}$$

In eq 4, k_1 and k_3 correspond to the reaction constants in Figure 3, $[E]$ is the enzyme concentration, $[H_2O_2]$ is the hydrogen peroxide concentration, and s is the ABTS

DOI: 10.1021/acsami.5b01884
ACS Appl. Mater. Interfaces 2015, 7, 14660−14669

concentration. In the defined equation, K is analogous to the Michaelis constant (K_M), and k equates to V_{max}/K, where V_{max} is the maximum rate of the reaction. Substituting eq 4 into eq 1 and making the aforementioned simplifications yields the following expression:

$$0 = D_S \frac{d^2 s}{dx^2} - \frac{ks}{1 + \frac{s}{K}} \quad (5)$$

This can be represented in the following dimensionless form:

$$0 = \frac{d^2 u}{d\chi^2} - \frac{\Phi^2 u}{1 + \alpha u} \quad (6)$$

where $u = (s/s_\infty)$, $\chi = (x/L)$, $\Phi^2 = (kL^2/D_s)$, and $\alpha = (s_\infty/K)$.

To our knowledge, no exact, closed-form solution of eq 6 has been published. However, it has been shown that, for large values of u, or when there is little substrate depletion, the following approximation can be made for eq 6:[57]

$$0 = \frac{d^2 u}{d\chi^2} - \frac{\Phi^2(\alpha + u)}{(1 + \alpha)^2} \quad (7)$$

Equation 7 can be solved to yield

$$u(\chi) = (1 + \alpha)\cosh\left(\frac{\sqrt{\Phi^2}\chi}{1 + \alpha}\right)\operatorname{sech}\left(\frac{\sqrt{\gamma\Phi^2}}{1 + \alpha}\right) - \alpha \quad (8)$$

and the flux, j, can be determined as

$$j = \alpha\left(\frac{du}{d\chi}\right)_{\chi=1} = \alpha\sqrt{\Phi^2}\tanh\left(\frac{\sqrt{\Phi^2}}{1 + \alpha}\right) \quad (9)$$

To understand the regime (reaction or diffusion limited) in which the catalytic films are operating, Φ^2 can be estimated using the following parameters: $k \approx 100\ s^{-1}$ (calculated from a known concentration of enzyme in the reaction solution and the theoretical limit of $k_{cat} \approx 10^{10}$ M/s), $L \approx 10^{-7}$ m (from the measured thickness of the film), and $D_s \approx 10^{-8}$ (m^2/s) estimated from the lower end of typical diffusion coefficients for small molecules through water scaled down by a factor of 1/3 from the assumption that the film is swollen with twice its volume in water. This assumption is based on the observation that the film swells to a deep magenta, corresponding to a film thickness of ~460 nm, when submersed in water. This yields an estimated Thiele modulus of $\Phi^2 \approx 10^{-3}$. Therefore, even for an enzyme that approaches the theoretical maximum enzymatic efficiency, the tested film is thin enough for the time scale for diffusion to be much faster than the time scale for reaction, and, in this case, we can reduce eq 9 using the approximation $\tanh[(\Phi^2)^{1/2}/(1 + \alpha)] \approx (\Phi^2)^{1/2}/(1 + \alpha)$ to yield the following equation:

$$j = \frac{\alpha\Phi^2}{1 + \alpha} \quad (10)$$

Equation 10 is simply the dimensionless Michaelis–Menten equation. The kinetic data from Figure 5 can be fit to this equation to extract the relevant kinetic parameters, shown in Table 2. The kinetic model with the fitted values for k_1 and k_3 is plotted in Figure 5. Despite immobilization and cross-linking of the protein, the bioconjugate retains 47% of the ABTS conversion activity of the free bioconjugate and 29% of the H_2O_2 binding activity.

Table 2. Kinetic and Transport Coefficients for Commercial Equine Heart Myoglobin, Recombinant Human Heart Myoglobin, Myoglobin Bioconjugate, and Catalyst Film

	k_1 (M^{-1} s^{-1})	k_3 (M^{-1} s^{-1})
eMb (solution)	173 ± 6.5	1800 ± 170
hMbC110A (solution)	72 ± 3.7	1100 ± 180
hMb–PNIPAM (solution)	213 ± 5.4	1500 ± 100
hMb–PNIPAM (film)	61 ± 1.8	700 ± 63

In addition to testing the bioconjugate coating on silicon, the robustness of this biocatalyst fabrication method was explored on a diverse selection of additional surfaces, including glass, polystyrene, and gold (an example conductive substrate). Films on each of the additional surfaces were cast using the same conditions as those on the silicon surface. The enzymatic activities of the bioconjugate catalysts on each of the surfaces, shown in Figure 6a, indicate that the catalysts all perform similarly, regardless of the underlying substrate. The wide range of support types that this material can be coated on while retaining high activity suggests that bioconjugate block copolymers have the potential to be useful in a variety of biocatalytic applications.

To evaluate the comparative effectiveness of this method for heterogeneous biocatalyst fabrication, the activity of the conjugate films was compared to three established enzyme immobilization techniques: LbL assembly,[25] covalent tethering on a reactive surface,[58] and encapsulation in polyurethane foam.[5,27] To provide the most relevant comparison between methods, the area of the catalytic coating was held constant at 0.25 cm^2. In the case of the block copolymer, LbL, and polyurethane films, the total enzyme contained in the catalyst was held constant at 6 $\mu g/cm^2$. Because the grafted protein monolayer is limited in enzyme density by the density of reactive groups or the required surface area per enzyme, the total enzyme content could not be similarly controlled for this immobilization method.

ABTS assays for all four catalyst preparation methods, shown in Figure 6b, indicate that the self-assembled conjugate films exhibit a 5–10-fold greater activity per protein than any of the other catalysts. The performance of the self-assembled conjugates, relative to the grafted film, is attributed to the fact that the method used to form the conjugate films allows for a large number of enzymes per unit area, because f the nanostructured packing of the protein. This allows for a higher catalyst density per unit area and improves the catalytic rate in the same manner, since nanostructuring is traditionally used to engineer heterogeneous catalysts from transition metals. The density of enzyme can be controlled both by changing the size of PNIPAM conjugated to the enzyme and by modulating the film thickness. The achievable density is primarily limited by needing to maintain a high enough viscosity to coat a stable film, as the unconjugated enzyme lacks the viscosity to form a coating. Coatability of this material is a major advantage for industrial applications, because it provides a simple, cost-effective method for fabricating catalysts using high-speed manufacturing processes on a variety of substrates.

In the case of LbL and polyurethane foams, high enzyme loadings per unit area can be achieved by varying film thickness, but the immobilization method introduces significant transport limitations that reduce the effective catalytic rate by making most of the enzyme inaccessible to substrate diffusion. Nanostructuring and a high degree of swelling in the self-

DOI: 10.1021/acsami.5b01884
ACS Appl. Mater. Interfaces 2015, 7, 14660–14669

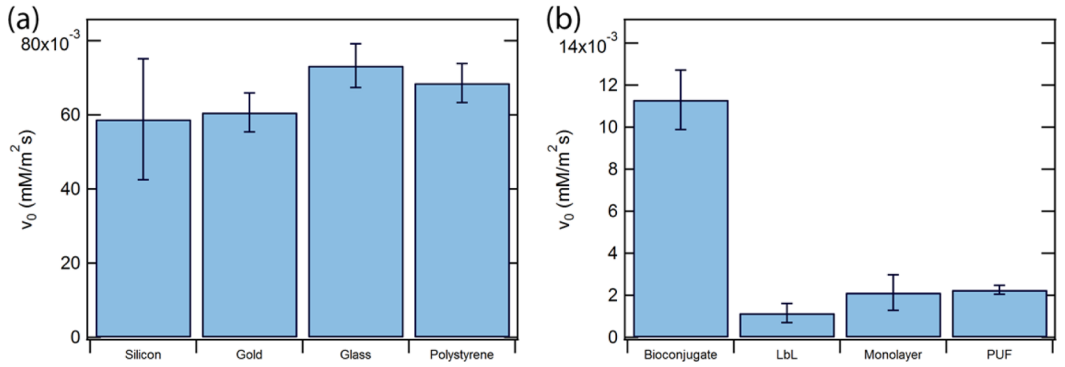

Figure 6. (a) Activity comparison between the bioconjugate coated on different supports indicates that the catalytic activity is largely independent of the support surface. (b) Activity comparison between the conjugate film and other immobilization techniques shows that the bioconjugate film exhibits over 5-fold greater activity than every other method.

assembled bioconjugate films provide paths for easy transport of substrates and products, which enables more rapid reaction. The dense packing of enzyme in the bioconjugate film also minimizes the distances over which transport is required, further limiting diffusional barriers to reaction. Therefore, self-assembled nanostructured catalysts can both improve protein packing density and reduce transport limitations, leading to significant improvements in biocatalyst performance.

In addition to catalyzing solution-phase oxidation reactions, the bioconjugate can also be used as a nitric oxide (NO) detector. NO sensors are useful in a variety of applications from measuring industrial pollutants to diagnosing respiratory inflammation. By coating hMb-PNIPAM onto a glass support, binding of NO to hMb can be tracked spectrophotometrically by a shift in the Soret absorbance band of the porphyrin ring (see Figure 7). Upon exposure to NO dissolved in solution at

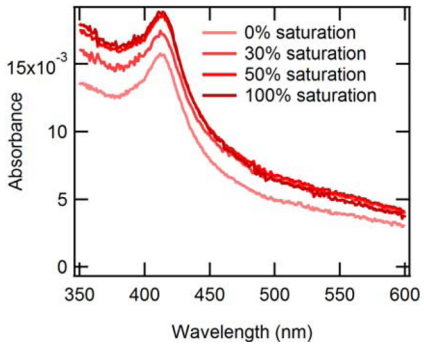

Figure 7. Nitric oxide detection assay shows a peak in the film which increases in absorbance as the film is exposed to higher amounts of NO.

30% saturation (~0.54 mM), 50% saturation (~0.9 mM), and 100% saturation (~1.8 mM) for 1 min each, a roughly linear increase in absorbance of the Soret band at 413 nm is observed as NO concentration increases from 0% saturation to 30% saturation, to 50% saturation.[59,60] Between 50% and 100% saturation of NO, little change is observed in absorbance. This is likely because the NO fully saturates the binding sites in myoglobin within the 1 min exposure time at these concentrations.

CONCLUSIONS

Myoglobin−-PNIPAM diblock copolymers provide a simple method for fabricating highly active biocatalytic films. Myoglobin can be efficiently bioconjugated with PNIPAM without significant change in the structure or activity of the protein, and the resulting block copolymers micro-phase-separate into weakly ordered lamellar domains at concentrations of 50 wt % and above. In comparison to previously studied bioconjugates, myoglobin conjugates are more poorly ordered, indicating that changes in protein structure can result in large changes in self-assembly behavior. The bioconjugate can be flow coated onto a silicon support to create uniform, catalytically active films with thicknesses of 100sn the order of hundreds of nanometers. These films do not form periodic nanostructures but rather show micro-phase separation with a characteristic feature size of 24 nm. Cross-linking these films using a glutaraldehyde fixative stabilizes the films and allows for heterogeneous catalysis of ABTS oxidation reactions, as well as for NO concentration measurements. The thinness of the film enables rapid diffusion of the reactive compounds, and a high degree of specific activity is retained for the protein. On a per-protein basis, the bioconjugate film performs 5−10 times better than catalysts made from other commonly used enzyme immobilization techniques. Therefore, controlling the nanostructure of enzymes using block copolymer self-assembly can potentially provide a powerful method for engineering transport properties and enzyme density in biocatalysts, yielding large improvements in catalyst performance.

METHODS

Bioconjugate Synthesis. Low-polydispersity poly(*N*-isopropylacrylamide) (PNIPAM) was synthesized by reversible addition−fragmentation chain transfer (RAFT) polymerization utilizing a maleimide-functionalized chain transfer agent (CTA), as reported previously.[36] The absolute molecular weight and polydispersity was determined by size-exclusion chromatography (SEC) on an Agilent Technologies 1260 Infinity system with a miniDAWN TREON MALS light scattering detector and a Wyatt Optilab T-rEX refractometer using *N*,*N*-dimethylformamide (DMF) with 0.02 M LiBr as the mobile phase.

The gene encoding human myoglobin variant hMbC110A (DNA Accession No. NM_203378.1) containing an additional N-terminal Cys residue and an N-terminal 6xHis tag was prepared for insertion into the bacterial T7-promoter expression vector pET15b by partial digestion with NdeI and *Bam*HI, producing a new plasmid: pET15b/hMb. The DNA and amino acid sequences for the gene are included in the Supporting Information. The recombinant expression plasmid was isolated from *Escherichia coli* (*E. coli*) NEB5α cells with selection for ampicillin resistance (100 μg/mL), and the correct constructs were verified by DNA sequence analysis. The expression plasmid pET15b/hMb was transformed into *E. coli* strain BL21star(DE3), and

DOI: 10.1021/acsami.5b01884
ACS Appl. Mater. Interfaces 2015, 7, 14660−14669

authenticity of the clones was confirmed by DNA sequencing. The *E. coli* were inoculated in culture tubes containing 5 mL of LB medium with 100 μg/mL ampicillin at 37 °C overnight. These starter cultures were then transferred to a 2.8 L Fernbach flask containing 1 L of LB medium and 100 μg/mL ampicillin. Cell growth was allowed to proceed at 37 °C for 10 h without induction. The cells were then harvested by centrifugation at 6000*g* for 15 min, yielding deep red pellets, which were stored at −80 °C until protein purification was commenced.

To purify the protein, frozen cell pellets were thawed and resuspended in lysis buffer (50 mM NaH_2PO_4, 300 mM sodium chloride, 10 mM imidazole, and 10 mM β-mercaptoethanol (BME), pH 8.0). Lysozyme was added to the suspension at a concentration of 100 mg/L initial culture, and the suspension was incubated at 4 °C for 1 h and sonicated. The lysate was clarified using centrifugation, and the protein contained in the supernatant fluid was purified using Ni-NTA metal affinity chromatography under native conditions. 2-Mercaptoethanol was added to each of the wash and elution buffers at a concentration of 10 mM to reduce disulfide bonds. The bright red elution fractions were dialyzed into 20 mM Tris-Cl buffer, pH 8.5, and were further purified using a HiTrap Q HP column (GE Healthcare, Uppsala, Sweden) in an AKTA FPLC machine using 20 mM Tris-Cl buffer, pH 8.5 as the mobile phase. The protein was eluted by introducing sodium chloride into the system at a concentration of 60 mM. Purity was assessed by taking absorbance readings at 280 nm, where there was a peak corresponding to Trp and Tyr residue absorbance, and 416 nm, corresponding to the peak for myoglobin Soret band absorbance in the buffer, on a Varian Cary 50 Bio UV/visible spectrophotometer. Fractions containing $A_{416}/A_{280} > 3.0$ were collected and combined. The purity of the protein was verified by denaturing gel electrophoresis (SDS-PAGE) (see Figure S5 in the Supporting Information). The yield of pure protein was typically ∼30 mg/L culture, measured spectrophotometrically at 280 nm with an extinction coefficient calculated based on the number of phenylalanine, tyrosine, tryptophan, and cysteine residues in the protein.

Purified human myoglobin was coupled to maleimide end-functionalized PNIPAM, using a maleimide−thiol coupling reaction, as described previously.[36] The resulting conjugate was precipitated three times in 1 M $(NH_4)_2SO_4$ with the last precipitation yielding a clear, colorless supernatant, indicative of the removal of all soluble, unconjugated myoglobin. The conjugate was then bound to Ni-NTA resin overnight and washed with 10 column volumes of wash buffer (50 mM NaH_2PO_4, 300 mM sodium chloride, 30 mM imidazole, pH 8.0) to remove the excess PNIPAM. The conjugate purity was assessed with denaturing SDS-PAGE with a broad band centered at ∼40 000 g/mol, corresponding to hMb-PNIPAM, and the final yield of the conjugate after purification was determined spectrophotometrically to be ∼30%. This final yield is similar to those obtained in other globular protein−polymer conjugations.[36,61] Enzymatic activity was compared to unconjugated hMb, revealing no detriment to the activity as a result of conjugation. The conjugate solution, dialyzed into pure water, was concentrated to ∼50 mg/mL, using Millipore Ultra-15 centrifugal filters with a molecular weight cutoff of 3 kDa. A portion of the concentrated solution was then formed into solid pellets by drop-casting aliquots onto a Teflon sheet and drying at room temperature overnight under vacuum.

Self-Assembly and Characterization. Bulk SAXS samples were formed by filling the center of a 1-mm-thick aluminum washer with the concentrated conjugate solution and drying the sample under vacuum at room temperature. This process was repeated until the center of the washer was almost filled by solid conjugate. Solution-state samples were formed by rehydrating the pellets to the desired concentration and transferring them into the washers. Both the bulk and solution-state samples were sealed with Kapton tape. The scattering patterns were obtained at Brookhaven National Synchrotron Light Source (NSLS) Beamline X27C. Samples were equilibrated for 10 min at each temperature before data acquisition. The collected data were corrected for empty cell and dark-field scattering.

DSC samples were prepared by loading 2−6 mg of bioconjugate solution into hermetically sealed aluminum pans. Data was acquired using a TA Instruments Discovery differential scanning calorimeter. Samples were equilibrated for 5 min at 5 °C, followed by two cycles of ramping to 40 °C at a rate of 10 °C/min, holding isothermally for 5 min, cooling to 4 °C at a rate of 10 °C/min, and holding isothermally for 5 min. The initial heating cycle was used to determine the transition temperatures.

Films were cast on all four different types of substrates from a 12 wt % solution under ambient conditions at a coating speed of 2.5 cm/min with a blade angle of 4° and a 127 μm separation between the blade and the substrate. The film dried quickly as it was cast, with the evaporation front lagging ∼1 cm behind the blade. The dry films were cured by immersion into 1.4 wt % glutaraldehyde in water at 45 °C to cross-link the myoglobin for 20 s. The cross-linked films were rinsed in deionized water for 20 s and dried under an air stream. Film thickness was measured for films cast on the Si substrate using a Woollam M-2000D spectroscopic ellipsometer. GISAXS patterns for these films on Si were obtained at the Cornell High Energy Synchrotron Source (CHESS) Beamline D1.

Samples for transmission electron microscopy (TEM) were prepared by casting a film as described above onto a silicon nitride TEM substrate with a membrane thickness of 20 nm and a window size of 100 μm × 100 μm. The samples were stained with ruthenium tetroxide vapors from a 0.5% aqueous solution for 20 min. Bright-field images were obtained on a FEI Technai TEM using an accelerating voltage of 120 kV and a LaB_6 filament.

Reaction Measurements. Initial reaction rates were measured *in situ* in polystyrene well-plates with a Tecan Infinite 200 PRO plate reader. All measurements were performed at 25 °C and mixed vigorously. The reaction solutions contained hydrogen peroxide and 2,2′-azino-bis(3-ethylbenzothiazoline-6-sulfonic acid) (ABTS) at concentrations varying from 5 μM to 1 mM in 50 mM sodium phosphate buffer, pH 6.0. Comparative tests were taken at an ABTS and hydrogen peroxide concentration of 100 μM each. Solution-phase measurements were performed at an enzyme concentration of 0.258 nM. Film activity measurements were performed by adhering 0.25 cm^2 films to the side of well plates with double-sided carbon tape to prevent obstruction of the beam path.

Three different methods were used to prepare films for comparing the catalytic activity of different films. First, to covalently bond an enzyme monolayer to the reactive polymer film, glass coverslips were cleaned by sequential sonication in acetone, methanol, and deionized water for 10 min each. These films were then amine-functionalized with 20 mM (3-aminopropyl)triethoxysilane in 90% isopropanol. A thin film of poly(ethylene-*alt*-maleic anhydride) (PEMA) was cast on a silicon substrate using a flow coater and cured at 120 °C for 2 h. After cooling, the film was rinsed with acetone, immersed in a 5 mg/mL solution of human myoglobin in 50 mM sodium phosphate buffer, pH 6.0, and incubated overnight at room temperature and then rinsed with deionized water.[58]

Layer-by-layer (LBL) films were prepared, following a method described by Lvov et al.[25] A glass microscope slide, cleaned by sequential sonication in acetone, methanol, 0.1 M NaOH, and deionized water for 10 min each, was used as the film support. The films were assembled by repeatedly, alternately immersing the substrate solutions of myoglobin and of poly(styrenesulfonate) (PSS) for 20 min per layer. The films were rinsed in deionized water for 1 min and dried under an air stream between each immersion. Both the myoglobin and PSS were at a concentration of 2 mg/mL in 50 mM phosphate buffer, pH 6.0, with 0.5 M sodium chloride. Protein content in the films was determined spectrophotometrically. The protein content was found to be linear with the number of bilayers, and six bilayers of myoglobin and PSS were needed to achieve the same protein quantity as in the conjugate film.

Polyurethane foams were prepared by combining polyurethane prepolymer HYPOL 3000 with a 5 mg/mL solution of myoglobin in 50 mM phosphate buffer, pH 6.0 at a 1:1 ratio.[27] The mixture was stirred vigorously for 30 s until homogeneous in appearance, and the resulting foams were cured at room temperature for 2 h. Samples for activity testing were prepared using a razor blade to slice thin pieces

DOI: 10.1021/acsami.5b01884
ACS Appl. Mater. Interfaces 2015, 7, 14660−14669

from the bulk foam. Protein content in the foams was determined by material balance.

NO detection was measured using hMb−PNIPAM film flow coated onto a glass microscope slide and cross-linked as previously described. A saturated NO solution made by dissolving 1.2 mM 1,1-diethyl-2-hydroxy-2-nitroso-hydrazine sodium in 50 mM phosphate buffer at pH 7.4. Solutions at 30% and 50% dissolved NO saturation where made by diluting the saturated solution with phosphate buffer. The films were soaked in the NO solutions for 1 min, dried with a paper towel, and absorbance spectra were taken immediately on a Varian Cary 50 Bio UV/visible spectrophotometer.

■ ASSOCIATED CONTENT

Ⓢ Supporting Information

Included in the Supporting Information is information on DNA and protein sequences for the myoglobin mutant, gels and UV-vis spectra showing purity of the protein and conjugate, GPC data on PNIPAM, additional SAXS, depolarized light scattering, turbidimetry, and DSC data on the conjugate, and stability data for the film. The Supporting Information is available free of charge on the ACS Publications website at DOI: 10.1021/acsami.5b01884.

■ AUTHOR INFORMATION

Corresponding Author

*E-mail: bdolsen@mit.edu.

Author Contributions

The manuscript was written through contributions of all authors. All authors have given approval to the final version of the manuscript.

Notes

The authors declare no competing financial interest.

■ ACKNOWLEDGMENTS

This work was supported by the Air Force Office of Scientific Research (Award No. FA9550-12-0259; thin film studies), the Department of Energy Office of Basic Energy Sciences (Award No. DE-SC0007106; bulk phase behavior), and the National Science Foundation (Award No. DMR-1253306; nitric oxide sensing assays). We thank Dr. Maya Koga for experimental assistance at NSLS beamline X27C at Brookhaven National Laboratory. We also thank Reginald Avery and Charlotte Stewart-Sloan assistance with data collection at CHESS, Dr. Carla Thomas for synthesis of PNIPAM, and we thank Dr. Jeremey Walker for generously providing us with a sample of HYPOL 3000. TEM micrographs were taken at MIT Center for Materials Science and Engineering. Ellipsometry and DSC were performed at the MIT Institute of Soldier Nanotechnologies.

■ REFERENCES

(1) Shimada, Y.; Watanabe, Y.; Sugihara, A.; Tominaga, Y. Enzymatic Alcoholysis for Biodiesel Fuel Production and Application of the Reaction to Oil Processing. *J. Mol. Catal. B: Enzym.* **2002**, *17*, 133−142.

(2) Hasan, F.; Shah, A. A.; Hameed, A. Industrial Applications of Microbial Lipases. *Enzyme Microb. Technol.* **2006**, *39*, 235−251.

(3) Mirjafari, P.; Asghari, K.; Mahinpey, N. Investigating the Application of Enzyme Carbonic Anhydrase for CO_2 Sequestration Purposes. *Ind. Eng. Chem. Res.* **2007**, *46*, 921−926.

(4) Dilmore, R.; Griffith, C.; Liu, Z.; Soong, Y.; Hedges, S. W.; Koepsel, R.; Ataai, M. Carbonic Anhydrase-Facilitated CO_2 Absorption with Polyacrylamide Buffering Bead Capture. *Int. J. Greenhouse Gas Control* **2009**, *3*, 401−410.

(5) Drevon, G. F.; Russell Alan, J. Irreversible Immobilization of Diisopropylfluorophosphatase in Polyurethane Polymers. *Biomacromolecules* **2000**, *1*, 571−576.

(6) Russell, A. J.; Berberich, J. A.; Drevon, G. F.; Koepsel, R. R. Biomaterials for Mediation of Chemical and Biological Warfare Agents. *Annu. Rev. Biomed. Eng.* **2003**, *5*, 1−27.

(7) Kim, M.; Gkikas, M.; Huang, A.; Kang, J. W.; Suthiwangcharoen, N.; Nagarajan, R.; Olsen, B. D. Enhanced Activity and Stability of Organophosphorus Hydrolase via Interaction with an Amphiphilic Polymer. *Chem. Commun.* **2014**, *50*, 5345−5348.

(8) Rahman, M. M.; Ahammad, A. J. S.; Jin, J. H.; Ahn, S. J.; Lee, J. J. A Comprehensive Review of Glucose Biosensors Based on Nanostructured Metal-Oxides. *Sensors* **2010**, *10*, 4855.

(9) Cass, A. E. G.; Davis, G.; Francis, G. D.; Hill, H. A. O.; Aston, W. J.; Higgins, I. J.; Plotkin, E. V.; Scott, L. D. L.; Turner, A. P. F. Ferrocene-Mediated Enzyme Electrode for Amperometric Determination of Glucose. *Anal. Chem.* **1984**, *56*, 667−671.

(10) Lojou, É.; Luo, X.; Brugna, M.; Candoni, N.; Dementin, S.; Giudici-Orticoni, M. T. Biocatalysts for Fuel Cells: Efficient Hydrogenase Orientation for H_2 Oxidation at Electrodes Modified with Carbon Nanotubes. *JBIC, J. Biol. Inorg. Chem.* **2008**, *13*, 1157−1167.

(11) Torchilin, V. P. Immobilised Enzymes as Drugs. *Adv. Drug Delivery Rev.* **1988**, *1*, 270.

(12) Luengo, J. M.; Alemany, M. T.; Salto, F.; Ramos, F.; Lopez-Nieto, M. J.; Martin, J. F. Direct Enzymatic Synthesis of Penicillin G Using Cyclases of Penicillium chrysogenum and Acremonium chrysogenum. *Nat. Biotechnol.* **1986**, *4*, 44−47.

(13) Bhosale, S. H.; Rao, M. B.; Deshpande, V. V. Molecular and Industrial Aspects of Glucose Isomerase. *Microbiol. Rev.* **1996**, *60*, 280−300.

(14) Ó'Fágáin, C. Enzyme Stabilization—Recent Experimental Progress. *Enzyme Microb. Technol.* **2003**, *33*, 137−149.

(15) Hanefeld, U.; Gardossi, L.; Magner, E. Understanding Enzyme Immobilisation. *Chem. Soc. Rev.* **2009**, *38*, 453−468.

(16) Minteer, S. D. *Enzyme Stabilization and Immobilization*; Humana Press: New York, 2010.

(17) Cracknell, J. A.; Vincent, K. A.; Armstrong, F. A. Enzymes as Working or Inspirational Electrocatalysts for Fuel Cells and Electrolysis. *Chem. Rev.* **2008**, *108*, 2439−2461.

(18) Mateo, C.; Palomo, J. M.; Fernandez-Lorente, G.; Guisan, J. M.; Fernandez-Lafuente, R. Improvement of Enzyme Activity, Stability and Selectivity via Immobilization Techniques. *Enzyme Microb. Technol.* **2007**, *40*, 1451−1463.

(19) Cloete, W. J.; Adriaanse, C.; Swart, P.; Klumperman, B. Facile Emmobilization of Enzymes on Electrospun Poly(styrene-alt-maleic anhydride) Nanofibres. *Polym. Chem.* **2011**, *2*, 1479−1481.

(20) Goldstein, L. Immobilized Enzymes: The Coupling of Biologically Active Proteins to Ethylene-Maleic Anhydride Copolymers of Different Anhydride Content. *Anal. Biochem.* **1972**, *50*, 40−46.

(21) Liu, C. Y.-C.; Rieben, N.; Iversen, L.; Sørensen, B. S.; Park, J.; Nygård, J.; Martinez, K. L. Specific and reversible immobilization of histidine-tagged proteins on functionalized silicon nanowires. *Nanotechnology* **2010**, *21*, 245105.

(22) Payne, C. M.; Resch, M. G.; Chen, L.; Crowley, M. F.; Himmel, M. E.; Taylor, L. E.; Sandgren, M.; Ståhlberg, J.; Stals, I.; Tan, Z.; Beckham, G. T. Glycosylated Linkers in Multimodular Lignocellulose-Degrading Enzymes Dynamically Bind to Cellulose. *Proc. Natl. Acad. Sci. U.S.A.* **2013**, *110*, 14646−14651.

(23) Nam, J.-M.; Han, S. W.; Lee, K.-B.; Liu, X.; Ratner, M. A.; Mirkin, C. A. Bioactive Protein Nanoarrays on Nickel Oxide Surfaces Formed by Dip-Pen Nanolithography. *Angew. Chem., Int. Ed.* **2004**, *43*, 1246−1249.

(24) Christman, K. L.; Enriquez-Rios, V. D.; Maynard, H. D. Nanopatterning proteins and peptides. *Soft Matter* **2006**, *2*, 928−939.

(25) Lvov, Y.; Ariga, K.; Ichinose, I.; Kunitake, T. Assembly of Multicomponent Protein Films by Means of Electrostatic Layer-by-Layer Adsorption. *J. Am. Chem. Soc.* **1995**, *117*, 6117−6123.

DOI: 10.1021/acsami.5b01884
ACS Appl. Mater. Interfaces 2015, 7, 14660−14669

(26) Caruso, F.; Trau, D.; Möhwald, H.; Renneberg, R. Enzyme Encapsulation in Layer-by-Layer Engineered Polymer Multilayer Capsules. *Langmuir* **2000**, *16*, 1485−1488.
(27) Hu, Z.-C.; Korus, R.; Stormo, K. Characterization of Immobilized Enzymes in Polyurethane Foams in a Dynamic Bed Reactor. *Appl. Microbiol. Biotechnol.* **1993**, *39*, 289−295.
(28) Sjoholm, K.; Cooney, M.; Minteer, S. Biocompatible Micellar Environment for Enzyme Encapsulation for Bioelectrocatalysis Applications. *ECS Trans.* **2009**, *19*, 1−7.
(29) Bates, F. S.; Fredrickson, G. H. Block Copolymers—Designer Soft Materials. *Phys. Today* **1999**, *52*, 32.
(30) Hamley, I. W. *Physics of Block Copolymers*; Oxford University Press; Oxford, U.K., 1998
(31) Park, C.; Yoon, J.; Thomas, E. L. Enabling Nanotechnology with Self Assembled Block Copolymer Patterns. *Polymer* **2003**, *44*, 6725.
(32) Olsen, B. D.; Segalman, R. A. Self-Assembly of Rod−Coil Block Copolymers. *Mater. Sci. Eng., R.* **2008**, *62*, 37−66.
(33) Lavigueur, C.; García, J. G.; Hendriks, L.; Hoogenboom, R.; Cornelissen, J. J. L. M.; Nolte, R. J. M. Thermoresponsive giant biohybrid amphiphiles. *Polym. Chem.* **2011**, *2*, 333.
(34) ten Cate, M. G. J.; Severin, N.; Börner, H. G. Self-Assembling Peptide−Polymer Conjugates Comprising (D-alt-L)-Cyclopeptides as Aggregator Domains. *Macromolecules* **2006**, *39*, 7831−7838.
(35) Olsen, B. D. Self-Assembly of Globular-Protein-Containing Block Copolymers. *Macromol. Chem. Phys.* **2013**, *214*, 1659−1668.
(36) Thomas, C. S.; Glassman, M. J.; Olsen, B. D. Solid-State Nanostructured Materials from Self-Assembly of a Globular Protein−Polymer Diblock Copolymer. *ACS Nano* **2011**, *5*, 5697−5707.
(37) Lam, C. N.; Kim, M.; Thomas, C. S.; Chang, D.; Sanoja, G. E.; Okwara, C. U.; Olsen, B. D. The Nature of Protein Interactions Governing Globular Protein−Polymer Block Copolymer Self-Assembly. *Biomacromolecules* **2014**, *15*, 1248−1258.
(38) Canalle, L. A.; Lowik, D. W. P. M.; van Hest, J. C. M. Polypeptide−polymer bioconjugates. *Chem. Soc. Rev.* **2010**, *39*, 329.
(39) Krishna, O. D.; Kiick, K. L. Protein- and peptide-modified synthetic polymeric biomaterials. *Pept. Sci.* **2010**, *94*, 32.
(40) Rabotyagova, O. S.; Cebe, P.; Kaplan, D. L. Protein-Based Block Copolymers. *Biomacromolecules* **2011**, *12*, 269.
(41) Lam, C. N.; Olsen, B. D. Phase transitions in concentrated solution self-assembly of globular protein-polymer block copolymers. *Soft Matter* **2013**, *9*, 2393−2402.
(42) Thomas, C. S.; Olsen, B. D. Coil fraction-dependent phase behaviour of a model globular protein-polymer diblock copolymer. *Soft Matter* **2014**, *10*, 3093−3102.
(43) Chang, D.; Lam, C. N.; Tang, S.; Olsen, B. D. Effect of Polymer Chemistry on Globular Protein−Polymer Block Copolymer Self-Assembly. *Polym. Chem.* **2014**, *5*, 4807−5186.
(44) Carlsen, C. U.; Skovgaard, I. M.; Skibsted, L. H. Pseudoperoxidase Activity of Myoglobin: Kinetics and Mechanism of the Peroxidase Cycle of Myoglobin with H_2O_2 and 2,2-Azino-bis(3-ethylbenzthiazoline-6-sulfonate) as Substrates. *J. Agric. Food Chem.* **2003**, *51*, 5815−5823.
(45) Everse, J.; Grisham, M. B.; Everse, K. E. *Peroxidases in Chemistry and Biology*; CRC Press: Boca Raton, FL, 1990; Vol. *1*.
(46) Veitch, N. C. Horseradish peroxidase: A modern view of a classic enzyme. *Phytochemistry* **2004**, *65*, 249−259.
(47) Romero, N.; Radi, R.; Linares, E.; Augusto, O.; Detweiler, C. D.; Mason, R. P.; Denicola, A. Reaction of Human Hemoglobin with Peroxynitrite: Isomeration to Nitrate and Secondary Formation of Protein Radical. *J. Biol. Chem.* **2003**, *278*, 44049−44057.
(48) Hubbard, S. R.; Hendrickson, W. A. X-ray Crystal Structure of a Recombinant Human Myoglobin Mutant at 2−8 Å Resolution. *J. Mol. Biol.* **1990**, *213*, 215−218.
(49) Witting, P. K.; Douglas, D. J.; Mauk, A. G. Reaction of Human Myoglobin and H_2O_2: Involvement of a Thiyl Radical Produced at Cysteine 110. *J. Biol. Chem.* **2000**, *275*, 20391−20398.
(50) Stephanopoulos, N.; Francis, M. B. Choosing an Effective Protein Bioconjugation Strategy. *Nat. Chem. Biol.* **2011**, *7*, 876−884.
(51) Mather, B. D.; Viswanathan, K.; Miller, K. M.; Long, T. E. Michael Addition Reactions in Macromolecular Design for Emerging Technologies. *Prog. Polym. Sci.* **2006**, *31*, 487−531.
(52) Obermeyer, A. C.; Olsen, B. D. Synthesis and Application of Protein-Containing Block Copolymers. *ACS Macro Lett.* **2015**, 101−110.
(53) Kalia, J.; Raines, R. T. Advances in Bioconjugation. *Curr. Org. Chem.* **2010**, *14*, 138−147.
(54) van Hest, J. C. M. Biosynthetic-Synthetic Polymer Conjugates. *Polym. Rev.* **2007**, *47*, 63−92.
(55) Romay, C.; Pascual, C.; Lissi, E. A. The Reaction Between ABTS Radical Cation and Antioxidants and its Use to Evaluate the Antioxidant Status of Serum Samples. *Braz. J. Med. Biol. Res.* **1996**, *29*, 175−183.
(56) Stafford, C. M.; Roskov, K. E.; Epps, T. H.; Fasolka, M. J. Generating Thickness Gradients of Thin Polymer Films via Flow Coating. *Rev. Sci. Instrum.* **2006**, *77*, 023908−023908−7.
(57) Lyons, M. E. G.; Greer, J. C.; Fitzgerald, C. A.; Bannon, T.; Barlett, P. N. Reaction/diffusion with Michaelis-Menten kinetics in electroactive polymer films. Part 1. The steady-state amperometric response. *Analyst* **1996**, *121*, 715−731.
(58) Cordeiro, A.; Pompe, T.; Salchert, K.; Werner, C. Enzyme Immobilization on Reactive Polymer Films. In *Bioconjugation Protocols*, Vol. *751*; Mark, S. S., Ed.; Humana Press: New York, 2011; pp 465−476.
(59) Zacharia, I.; Deen, W. Diffusivity and Solubility of Nitric Oxide in Water and Saline. *Ann. Biomed. Eng.* **2005**, *33*, 214−222.
(60) Antonini, E.; Brunori, M. *Hemoglobin and Myoglobin in Their Reactions with Ligands*; North-Holland Publishing Co.: Amsterdam, 1971.
(61) Bays, E.; Tao, L.; Chang, C. W.; Maynard, H. D. Synthesis of Semitelechelic Maleimide Poly(PEGA) for Protein Conjugation by RAFT Polymerization. *Biomacromolecules* **2009**, *10*, 1777.

DOI: 10.1021/acsami.5b01884
ACS Appl. Mater. Interfaces 2015, 7, 14660−14669